iScience

CellPress
OPEN ACCESS

Article

Lifetime of glass nanopores in a PDMS chip for single-molecule sensing

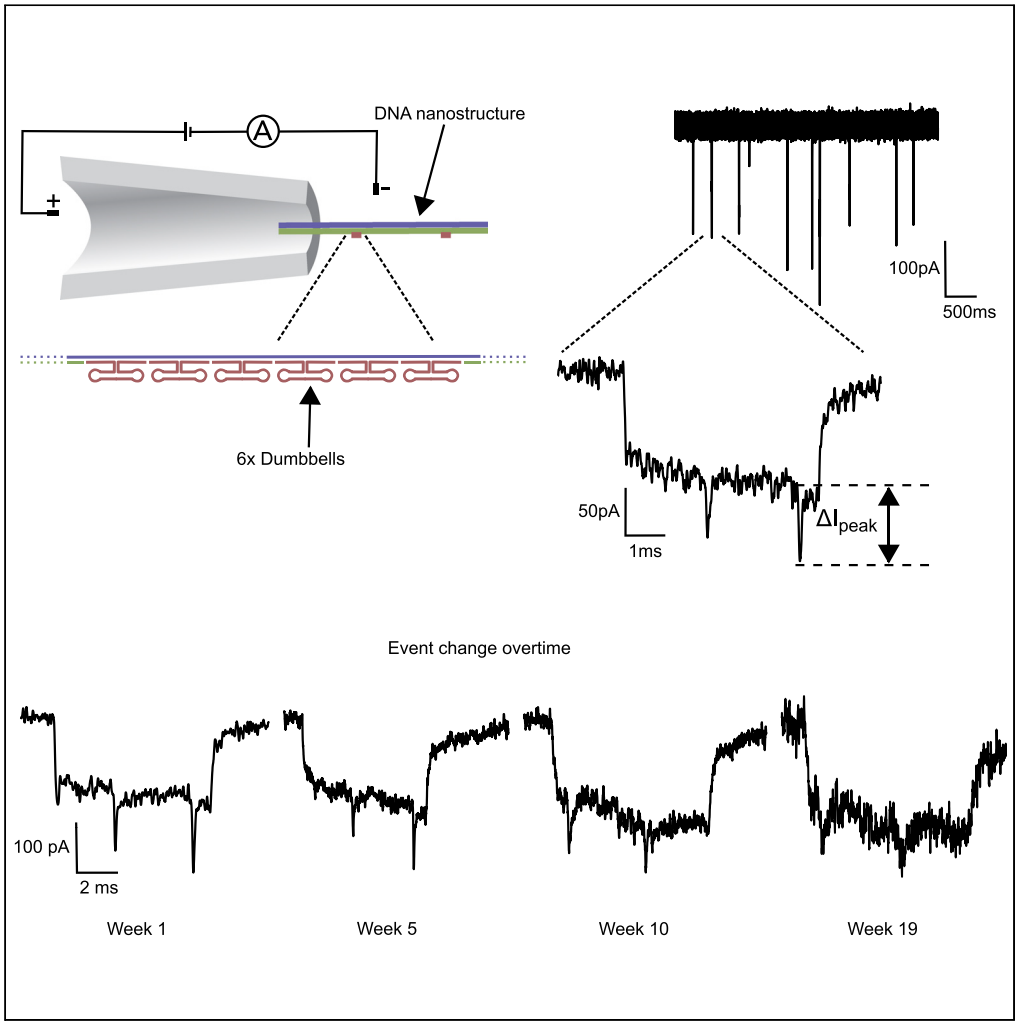

Mohammed F. Alawami, Filip Bošković, Jinbo Zhu, Kaikai Chen, Sarah E. Sandler, Ulrich F. Keyser

ufk20@cam.ac.uk

Highlights

Maintaining low noise and linear current-voltage relation is crucial for biosensing

Multiple nanopores embedded in a chip can make more than 90 different measurements

Nanopores can be reused weekly over 19 weeks

Nanopore failure can be attributed to contaminant accumulation and dissolution

Alawami et al., iScience *25*, 104191
May 20, 2022
https://doi.org/10.1016/j.isci.2022.104191

iScience

CellPress
OPEN ACCESS

Article

Lifetime of glass nanopores in a PDMS chip for single-molecule sensing

Mohammed F. Alawami,[1,2] Filip Bošković,[1] Jinbo Zhu,[1] Kaikai Chen,[1,2] Sarah E. Sandler,[1] and Ulrich F. Keyser[1,2,3,*]

SUMMARY

Nanopore sensing is an emerging technology that has many biosensing applications ranging from DNA sequencing using biological pores to biomolecular analysis using solid-state pores. Solid-state nanopores that are more stable are an attractive choice for biosensing applications. Still, biomolecule interactions with the nanopore surface reduce nanopore stability and increase usage costs. In this study, we investigated the biosensing capability for 102 quartz glass nanopores with a diameter of 11–18 nm that were fabricated using laser-assisted capillary pulling. Nanopores were assembled into multiple microfluidic chips that were repeatedly used for up to 19 weeks. We find that using vacuum storage combined with minimal washing steps improved the number of use cycles for nanopores. The single-molecule biosensing capability over repeated use cycles was demonstrated by quantitative analysis of a DNA carrier designed for detection of short single-stranded DNA oligonucleotides.

INTRODUCTION

Solid-state nanopores are one promising single-molecule sensing method that makes them an attractive choice for biosensing. The popularity of solid-state nanopores in lab settings stems from their ease of size adjustability, their stability in almost any environmental condition, and the ability to fabricate them using different materials and methods (Xue et al., 2020). One of the easiest, and potentially cheapest, methods of fabricating nanopores is the laser-assisted pulling of a glass capillary to make two nanopores, which can be used to make multi-nanopore chips (Bell et al., 2013).

The principle of this technology is based on resistive pulse sensing where a nanopore is placed between two electrolyte-filled chambers (Bezrukov, 2000). A voltage is applied across the nanopore to drive molecules from one chamber to another. When a molecule translocates across the nanopore, the ionic current changes corresponding with its size, charge, and structure (Figure 1). For example, it can be used to measure the length of double-stranded DNA (dsDNA) or read a barcode that is imprinted on dsDNA for gene profiling and fingerprinting applications (Albrecht, 2017; Dekker, 2007). Nonetheless, solid-state nanopores sensing has key limitations which include the inherent lack of specificity that can be addressed by multiple approaches, e.g., by modifying nanopores, incorporating new sensing modalities to them, or designing probes that are specific to the targeted biomolecules (Xue et al., 2020). Different principles can be used to utilize DNA nanostructures for detecting the presence of the desired molecules and quantifying their concentration (Bell and Keyser, 2016, Beamish et al., 2020; Cai et al., 2021; Charron et al., 2019; Nouri et al., 2019).

One other major limitation with nanopores is the perceived need to modify the surface to increase its lifetime. Most of the publications we found looked into increasing the lifetime of nanopores by coating nanopores with polymers, hafnium oxide, peptides, or polyethylene glycol (Awasthi et al., 2020; Chou et al., 2020; Karmi et al., 2020; Roman et al., 2017). This shows that studies on increasing the lifetime of nanopores are still limited. To the best of our knowledge, only a few groups have investigated the reusability in detail, but none examined conical glass nanopores (Chou et al., 2020; Karmi et al., 2020; Roman et al., 2017; Van den Hout et al., 2010). Chou et al., 2020 showed that different storing solutions can improve the stability of nanopores over time but with time the diameter of nanopores increases which affects the stability of nanopores. To improve stability, nanopores were coated with single digits nm-thick hafnium oxide to reduce nanopore expansion, but the benefit can last only a few days in salt solutions (Chou et al., 2020). Expansion

[1]Cavendish Laboratory, University of Cambridge, JJ Thomson Avenue, Cambridge CB3 0HE, UK

[2]Cambridge Nucleomics, 254 Turning Way, Cambridge CB3 1AF, UK

[3]Lead contact

*Correspondence: ufk20@cam.ac.uk

https://doi.org/10.1016/j.isci.2022.104191

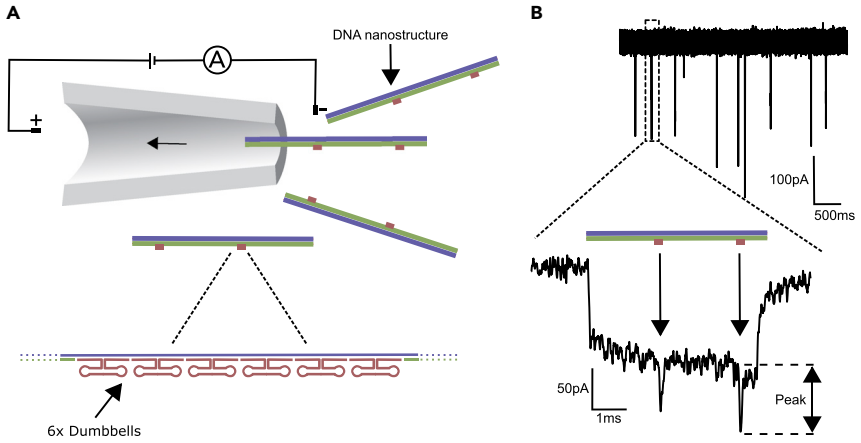

Figure 1. Principle of nanopore sensing

(A) Schematic illustration for detecting DNA carriers. The DNA carrier is a double-stranded DNA carrier made by assembling a 7228-nucleotide long M13mp18 ssDNA scaffold and complementary staples. Two wider structures are incorporated along with the DNA; each is made from 6 x DNA double-hairpin (DNA dumbbells). The DNA carrier is driven through the nanopore by the applied electric field.

(B) An example for an ionic current trace (top) and a typical DNA carrier translocation event (bottom) is shown. Each 6 x DNA dumbbell structure blocks more volume of ions than the dsDNA during translocation resulting in the second drop of current which is observable as two peaks as indicated with arrows.

of the nanopore diameter reduces their sensitivity which affects the reproducibility for the analysis of biomolecules. Another study has utilized peptide-coating of silicon nitride nanopore surfaces to increase their life for up to 7 months (Karmi et al., 2020). Awasthi et al., 2020 showed reduced clogging after polymer coating due to less protein absorption, but RMS increased, and events looked significantly different after coating. Karmi et al., 2020 showed evidence for an increase in current stability and reduced background noise after coating, but here also events over time were not investigated. Chou et al., 2020 have only considered the current characteristics as a measure of nanopore performance.

Other earlier strategies to improve nanopore stability and reduce the expansion of nanopores diameter in salt solution utilized nanopore fabrication to make nanopore shapes that can have higher stability (Van den Hout et al., 2010). This can be achieved by using a drilling TEM beam that matches the desired nanopore diameter.

Enclosing nanopores in a microfluidic chip can also help in maintaining their reusability for a longer time by reducing evaporation (Roman et al., 2017). Roman et al., 2017 also coated solid-state nanopores with polyethylene glycol to protect nanopores and enable long-term measurements, but biosensing over time was not investigated.

The literature presented above shows the need for studying the stability of conical glass nanopores chips including their ability to detect molecular structures for single-molecule sensing. The sensitivity and reliability of nanopores change over time due to contamination and possible nanopore partial clogging, breakage, or dissolution, which can limit the reusability of the nanopores (Awasthi et al., 2020; Chou et al., 2020); subsequently, it also increases the average cost and preparation time per measurement. Thus, quantification of the number of distinct measurements that are possible for unmodified glass nanopores is a crucial element for the large adoption and commercialization of nanopore sensing while keeping the sensing principle as general as possible.

Here, we investigated multiple nanopores assembled into a PDMS chip. We used a straightforward cleaning and storage protocol to extend the lifetime of nanopores without any surface modification. We show the lifetime by reusing seven chips, each having 12–14 nanopores, measured weekly over 19 weeks. The functionality of nanopores based on current-voltage (IV) characteristics and the signal of translocating DNA molecules was measured. To determine if the nanopores are still capable of single-molecule analysis for quantifying biomolecules, the concentration of short oligonucleotides was measured and compared in fresh and two-week-old chips. The results indicated that nanopore chips can be reused weekly over 19 weeks for

biosensing after enclosing them in a PDMS chip with a combination of washing and storing of the nanopore chips. The result of this work establishes the repeated usability of unmodified glass nanopores with a straightforward storage process that can be easily adapted to the needs of specific biosensing applications.

RESULTS AND DISCUSSION

Biosensing principle

To investigate the biosensing capability of nanopores, we made a well-established DNA carrier sample introduced in our previous studies that can be used to study the signal-to-noise ratio (SNR) in translocation events (Bell and Keyser, 2016) (Figures 1A and S1D). A single-stranded DNA molecule (ssDNA) was hybridized with complementary short ssDNA sequences and DNA dumbbells nanostructures to make a dsDNA carrier that produces two signal levels that represent DNA baseline and two peaks—each peak corresponds to 6 x dumbbell nanostructure (Figure 1B). This DNA carrier was used to study the biosensing capability of the nanopores over 19 weeks.

Nanopore fabrication and testing over time

We fabricated 102 conical nanopores with diameters ranging from 11–18 nm using a laser-assisted capillary puller as previously described (Bell and Keyser, 2016). The fabricated nanopores were used to assemble eight chips with 12–14 nanopores per chip, seven chips were used for weekly measurements, and one chip for daily measurements (Figures 2A and S3–S18). After plasma treatment and filling the chips with nanopore measurement buffer (4M LiCl, 1xTE, pH$\sim$ 9.4), the IV curve and current root-mean-square (RMS) of the baseline at voltage 600 mV at a bandwidth of 50 kHz were measured to determine the number of working and biosensing nanopores. We define a working nanopore as a pore that has a linear IV relationship but has RMS above 8 pA (Figures S1A and S1C). A biosensing nanopore, on the other hand, has a linear IV relationship and a baseline RMS below 8 pA (Figures S1A and S1B) and can be used for DNA structure analysis. It is important to note that one earlier report considered a nanopore to be functional based on only ionic current characteristics (Chou et al., 2020). In contrast, we believe that the key metric for successful biosensing purposes is successful structure analysis of single biomolecules. It is worth noting that the baseline RMS cut-off value here is specific for our application with six dumbbell structures (Figure 1A). Sensing of larger structures can be done even at higher RMS depending on the magnitude of the secondary peak.

Before we introduce our storage protocol, we will briefly review the reasons for nanopores' failure. There are several reasons why the number of working/biosensing pores can be lower than the fabricated ones. The number of working/biosensing nanopores is always lower than the fabricated nanopores due to the loss of nanopores during manual chip fabrication. In addition, randomness in the pulling process may result in producing smaller or larger diameter nanopores than required for the current experiment. Incomplete filling with buffer due to low wettability is another well known effect that can limit the number of working nanopores. To enable the reusability of nanopores over the long term, we assembled nanopores in a PDMS chip and followed that with a washing and sealing protocol to prevent evaporation and reduce contamination from previous samples, see Figure 2A. Initially, each chip's loading chamber was washed twice with nanopore measurement buffer, then vacuum-sealed after each measurement.

We start by discussing the number of nanopore chips that work. Based on the definition of working and biosensing nanopores, a working chip is defined as a chip that has at least one working nanopore, and a biosensing chip has at least one biosensing nanopore. Figure 2B shows that in week one all seven nanopore chips are working and biosensing. The number of usable chips fluctuated until all chips failed after week 19. Having looked at nanopore chips, we now investigate the individual working and biosensing nanopores as a function of weeks in Figures 2C and 2D. We show the ratio of nanopores per chip to make the data comparable. In general, we observe that nanopores stop working on the same timescale as expected from Figure 2B for the chips. It is important to note that the error bars indicate the variability between different nanopore chips which indicates the randomness of the filling process and failure of the nanopores.

We assessed the effectiveness of our sealing protocol on the functionality of the nanopores by testing a single chip with 14 nanopores that were just washed and stored on a bench over days without sealing. Our results of daily single-molecule measurements over 4 days are shown in Figure 2E. On the fourth day of measurement, there was only one working nanopore left that was not fit for biosensing. These results demonstrate that our sealing protocol is essential to extend the reusability of nanopores to up to 19 weeks or a factor of 30.

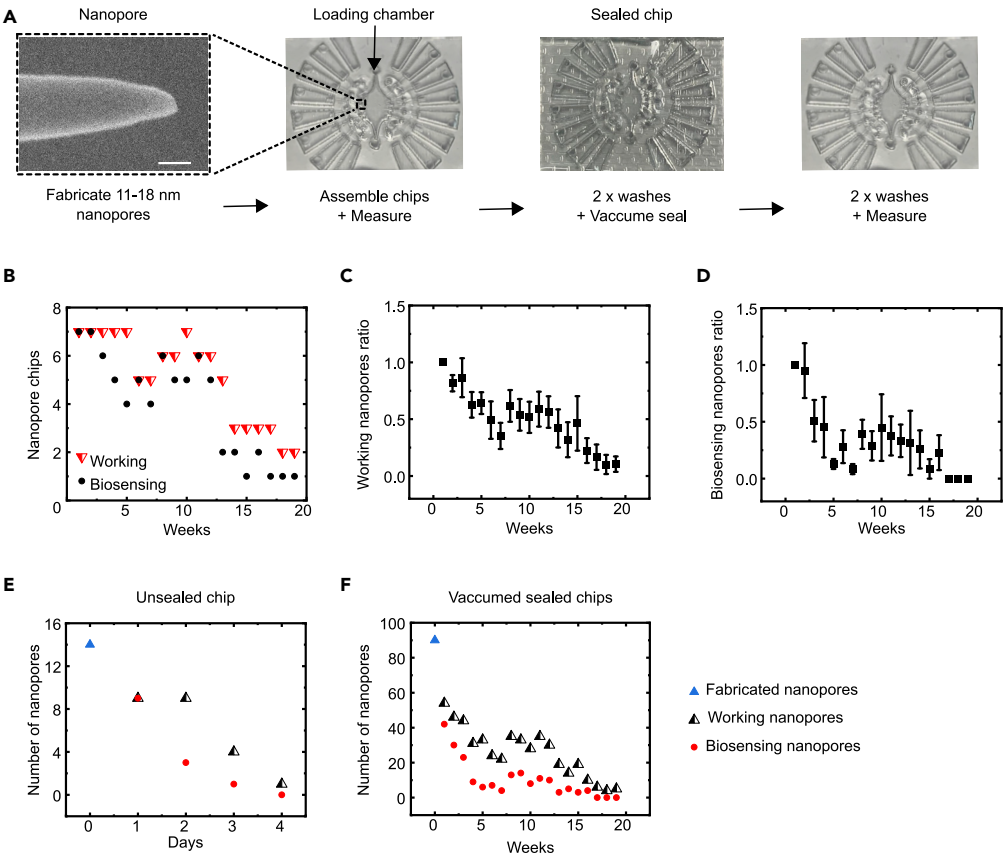

Figure 2. The lifetime of nanopores

(A) Illustration of the storage process. After the chip is assembled and used for measurement, the chip's loading chamber (indicated with an arrow) is washed twice with nanopore measurement buffer (see STAR Methods for more details), then vacuum sealed and stored. Before reusing the chip, the chip's loading chamber is washed twice with the same buffer. Scale bar = 100 nm. (b–d) Vacuum-sealed chips.

(B) Number of functional chips over time. Working chips have at least one working nanopore with a linear current-voltage (IV) curve and a root-mean-square (RMS) above 8 pA. Biosensing chips have at least one biosensing nanopore with a linear IV relationship and RMS below 8 pA.

(C) Ratio of working nanopores in vacuum-sealed chips over 19 weeks (n = 7).

(D) The ratio of biosensing nanopores over 19 weeks (n = 7).

(E) Number of functional nanopores without vacuum-sealing over 4 days.

(F) The number of functional nanopores with vacuum-sealing over 19 weeks. Error bars correspond to the SE of the mean (±SEM). The buffer used in all experiments is 4 M LiCl, one x TE, pH ~ 9.4.

We now return to the raw numbers of working nanopores over the seven chips. Our data show that the number of biosensing nanopores is lower than working nanopores (Figure 2F). Figure 2F also shows that the total number of biosensing nanopore drops quickly to less than five on week 7 (red symbols, Figure 2F). We hypothesized that the rapid decline might be explained by random changes in nanopore buffer filling, possible air bubbles (Smeets et al., 2006), and accumulation of contamination in the sample chambers (Smeets et al., 2008). Owing to the marked reduction of working and biosensing nanopores by week 7, we decided that the accumulation of contamination, which causes nanopore clogging, could be the main reason. Here, we define clogging as the long/persistent reduction of current to values near zero nA (Figures S3 and S5). Hence, we introduced more washing steps starting from week eight before each new measurement. The increase to a total of four washes after each use markedly increased the number of recovered nanopores from week 8 (Figures 2C, 2D, and 2F). The extra washes (in weeks 8–19) resulted in recovering two nanopores per chip on average and in the recovery of two biosensing chips (Figures 2B–2D).

Following this insight, we quantified any remaining contamination after repeated usage of our chips as well. Using the original protocol, a chip loading chamber was washed twice after measuring a DNA sample and

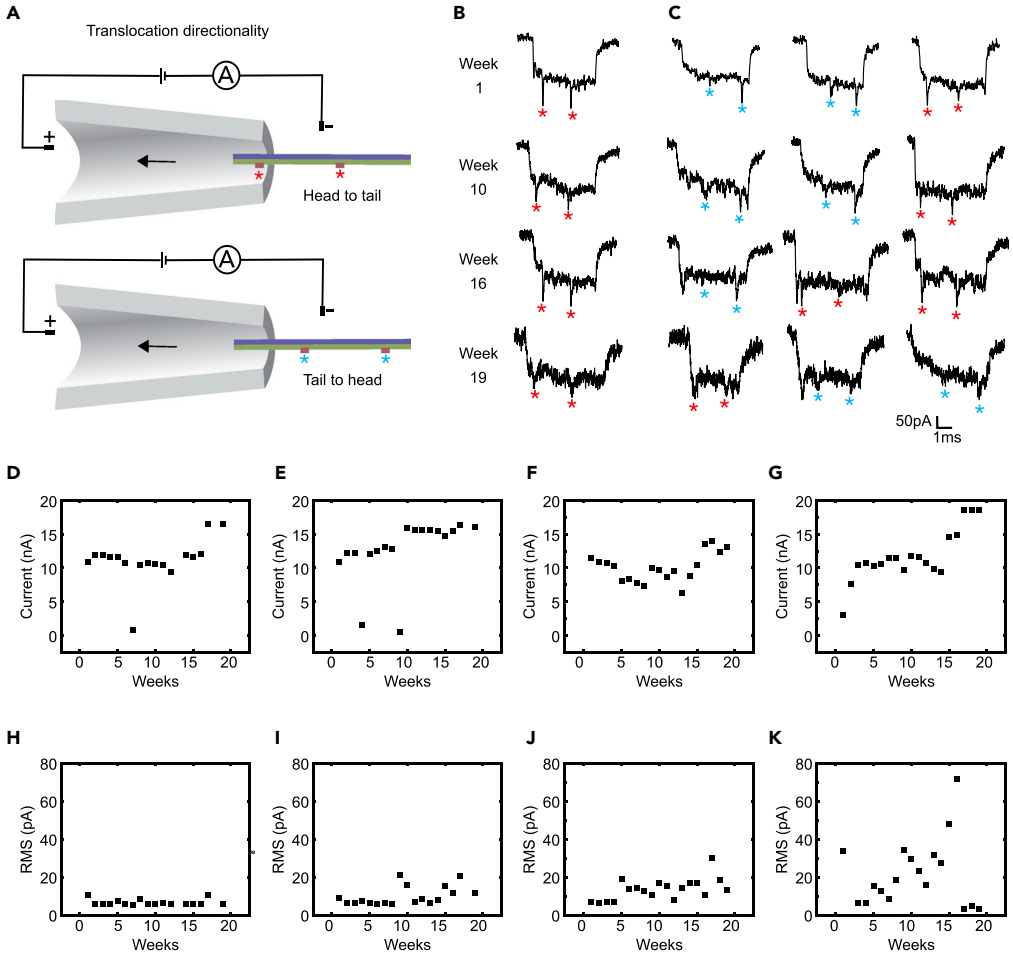

Figure 3. Examples of nanopore characteristics over 19 weeks

(A) DNA carrier translocates in two directions namely: (top) head to tail, and (bottom) tail to head.

(B) Peaks can still be distinguished from normal DNA levels over 19 weeks. Example of typical DNA carrier events from weeks 1, 10, 16, and 19, respectively (more detail in Figure S7). Different nanopores are used to make measurements in the same chip.

(C) The first three unfolded or partially folded events from weeks 1, 10, 16, and 19. The results show a decrease in signal-to-noise ratio (SNR) over time (more detail in Figure S1D). Asterisk (*) peaks corresponding to the DNA dumbbells nanostructures.

(D–G) Examples for ionic current at 600 mV over 19 weeks. (H–K) Examples of current baseline RMS at 600 mV over 19 weeks. The buffer used in all experiments is 4 M LiCl, one x TE, pH ~ 9.4.

refilled with a fresh measurement buffer. We then monitored the ionic current and detected approximately four events per hour at 600 mV. Considering the average events per measurement are 1260 events per hour at 600 mV in our experiments, we reduced the background events to around 0.3%. The residual detection of the sample indicated that the two washing steps were enough to reduce the remaining concentration of biomolecules by more than 99% but a larger sample concentration remaining may explain the loss of nanopores until week 7. The additional washing steps reduced the remaining sample and hence reduced clogging of nanopores and likely explain the increase of working/biosensing nanopores after week 7.

Another key parameter for biosensors is the current RMS fluctuations of the baseline. Figure 3A shows the two possible translocation directions head-to-tail or tail-to-head. Typical translocation events in head-to-tail are shown in Figure 3B for weeks 1, 10, 16, and 19. In Figure 3C, we show the first three unfolded events in a few nanopores. The additional peaks due to the dumbbells are observable. We use the average baseline at the start of the measurement with an external filter frequency of 50 kHz and a sampling frequency of 1 MHz to calculate the RMS. During our measurements, we found that for any RMS above 8 pA, the second

drop in the DNA event from the dumbbell structure becomes harder to distinguish from the DNA current drop (Figures 3B, 3C, and S1D). Thus, we set a threshold of 8 pA to ensure sufficient distinguishability of DNA dumbbell nanostructures to use nanopores for single-molecule detection as used to define a biosensing nanopore (see above). The 8 pA value was chosen to make the data analysis with a custom-written data analysis program that uses a static threshold. More sophisticated analysis procedures including machine learning approaches could be employed. However, we decided to work with the solution that uses the simplest possible data analysis approach, high SNR, and thresholding.

Events from all measurements were analyzed to determine the effect of storage on the distinguishability of the secondary iconic drops from the DNA primary current drop. Peaks were still distinguishable until week 19, even with the increase in baseline RMS (Figure 3C). Events with fully intact DNA carriers were observed until week 19 (Figures 3B and S7). This result indicates that detecting DNA carriers can still be done even at moderately increased RMS with chips that have been used weekly for 19 weeks to make 19 measurements. It is worth noting here that due to the random behavior of nanopores from one week to another, different nanopores from each chip were used for measurement across the different weeks. Some of the nanopores have a different current baseline and hence shape and diameter. The difference in nanopores' characteristics leads to changes in the signal across some of the measurements.

To determine the number of distinct measurements that can be done using nanopore chips, a short-term experiment was conducted. A 12-nanopore chip was used to make 21 individual nanopore measurements for a total of 252 measurements over 6 days, and out of those, 95 measurements showed successful translocation events (Figures S9–S17, Table S2). Nanopore could make 20 distinct measurements over 6 days, which is comparable to the number of measurements achieved during the weekly experiment.

Interestingly, the combined daily and weekly results show that long-term repeated usability can result in enlarging the nanopores. For the 19-week measurements, we found that many nanopores failed after having a higher current (Figures S5 and S8), which is consistent with what was reported in the literature where nanopores increased in diameter in 1M KCl, 1M MgCl2, and 1M LiCl (Chou et al., 2020). In contrast, the majority of nanopores failed due to clogging or reduction in current for the short-term daily measurements (Figures S9–S17).

Another reason for pore failure other than pore enlargement and clogging is the increase in pore baseline current RMS. This could be due to contaminant interaction with the pore surface at the entrance, which we noticed can be sometimes cleared by reversing the voltage momentarily (Figure S5J). This can act as a pushing-out mechanism of contaminants. Sometimes, the effect cannot be reversed which causes a permanent pore failure (Figure S5N). We have also noticed that the more the chip is reused, the more difficult it is to reverse the clogging. This might be due to the accumulation of contaminant that forms structures bound to the surface of the nanopore, and the applied voltage is not sufficient to break the bonding or release the contaminants.

Other than the distinguishability of the peak's signals from the DNA current drop level, the current baseline level, its RMS and the event characteristics were investigated (Figures 3D–3K and S3–S8). The level of baseline current indicates the size of the nanopore; hence, the increase in current over time could be correlated with an increase in the nanopore diameter size. Larger nanopores with baseline currents of 18 nA and above are too large to detect the DNA secondary structure on DNA carriers and hence were considered unfunctional. Moreover, the increase in current and RMS is associated with less distinguishability between the DNA dumbbell peaks and the DNA baseline current. The general trend in all the nanopores is that both baseline current and RMS increase over time (Figures 3D–3K). Here again, we observe inter-nanopore variability as some nanopores sustained their RMS and current over many weeks, while others increased after a few measurements. The reasons for the variability are again changes in wettability, breakage of a nanopore, or random contamination accumulation.

The most crucial aspect for biosensing from this experiment was found to be the baseline current RMS level. Figures 3H–3K show four-time series for four nanopores over the full observation time of 19 weeks. When the level is below 8 pA, the six x dumbbell peaks become easily distinguishable even after weeks of usage. Maintaining nanopores with RMS below 8 pA is more challenging than maintaining working nanopores. We observed that for the majority of nanopores, their baseline RMS increased after repeated usage even when these nanopores were not used for DNA measurements.

Overall, even with the increase in both current and baseline RMS, the detection of the dumbbell groups on the DNA carrier was achieved (Figures 3B and 3C). Further cleaning of nanopores, removing of contamination, and gentle handling of the chip resulted in maintaining a stable level of current and low enough baseline RMS to more than 19 weeks. The utilization of a cleanroom to reduce aerosols, ensuring complete crosslinking of PDMS, the use of clean (filtered) buffers, and using sterilized new tubes could further reduce the contamination that results in the clogging of nanopores.

Effect on biosensing in reused nanopores

As mentioned previously, nanopore sensing has a huge potential in sensing biomolecules, but the limited detection specificity makes it difficult to use them directly. One approach to increase the specificity of nanopores is to use short DNA oligos for coating the surface of the nanopore (Iqbal et al., 2007; Nilsson et al., 2006). Another method that does not require coating nanopores is to design a DNA probe that can be used to specifically detect the short molecule of interest (Bell and Keyser, 2016). For example, barcoded DNA carriers with protein-binding sites can be used to detect different proteins simultaneously (Bell and Keyser, 2016). The same principle in combination with strand displacement can also be used to detect SNP in short DNA oligos and measure their concentration (Kong et al., 2017). Here, we further improved the DNA carrier design to detect a larger dynamic range of concentration for short DNA oligos. We repeated the concentration measurements over two weeks and compared results from both reused and fresh chips to determine the effect of repeated use on quantifying biomolecules. Extended washing steps were also performed to maximize the lifetime of the chip.

We designed a DNA carrier with five sensing sites that are complementary to a DNA target comprised of 20 nucleotides (nt) (Figure 4A). A 14 nt streptavidin-biotin-labeled DNA probe (SBP) was used to partially bind to the sensing sites (Figure 4B). When the target DNA is present, all SBP probes on the five sensing sites will be displaced by the target DNA (Figure 4C). The target strand is fully complementary to the overhang at the sensing sites; hence, the net gain in the six more base pairs than SBP will thermodynamically drive the strand displacement reaction forward resulting in the dissociation of SBP (Zhang and Winfree, 2009). Because the 20-base pair DNA duplex left at the sensing site is much smaller than the SBP, the SBP peak disappears. This results in a loss of signal that corresponds with the detection of the targeted oligo.

As introduced before, we use two groups of six x dumbbell structures on the DNA carrier at the two ends of the sensing area as references. The presence of the peaks ensures that we can detect the presence or absence of the additional peaks. Each 6 x dumbbell structure produces a peak signal that is comparable, in terms of size and magnitude, to the SBP probe (Chen et al., 2020). Thus, this structure can be also used to confirm the presence of SBP and gives sufficient SNR for positive target detection.

We can determine the concentration of the target strand by counting the number of absent peaks due to the presence of the target strand (Figures 4D–4F) as described earlier (Kong et al., 2017). When no target is added, the number of peaks should be at maximum (Figure 4D). When the concentration of the target oligo is high, the majority of the SBP probes are displaced; hence, most of the measured events would only have the reference peaks (Figure 4E).

Seven different concentrations of short DNA target were measured individually ranging from 500 pM to 250 nM using fresh chips (Figure 4F, Table S1). We report the ratio of the peaks, which is the total number of peaks divided by the total number of analyzable events. The peak ratio represents a direct measure of the concentration of DNA target strand present in each sample. The results in Figure 4F show that the method can detect the concentration with a dynamic range of up to three orders of magnitudes. Further addition of sensing sites could help in further increasing the sensitive dynamic range of target concentration. A similar method can be employed for the identification of proteins or any other biomolecule with a specific sensing site on the DNA carrier.

Next, the effect of using reused chips for quantifying short oligos was investigated. A two-week-old chip was compared to a freshly made chip. In Figure 4G, the data from the two chips yield similar results, which indicate the reliability of the chip processed by the storage and cleaning method. The concentration calculated using an old chip was slightly lower than the one obtained from the fresh chip, which could be due to higher RMS after multiple measurements, as demonstrated in Figure 3. Interestingly, when the relationship

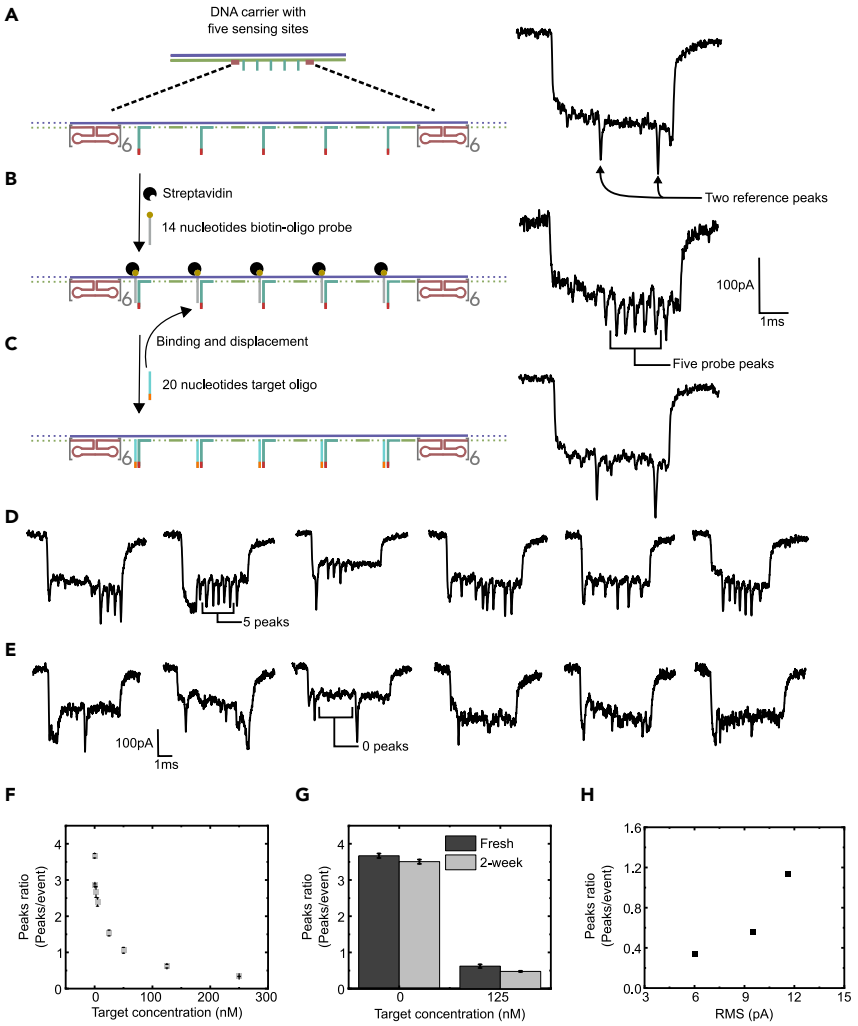

Figure 4. Measuring target concentration with nanopore sensing

(A–C) Schematic illustration of DNA strand displacement reaction on the DNA carrier. (A) Five sensing sites with 20 nt overhang complementary to the target are designed between two groups of referenced structures on the carrier. (B) 14 nt biotin-oligo probe is used to partially bind to the five binding sites. Monovalent streptavidin is used to amplify the biotin-oligo probe signal. (C) 20 nt target oligo is added to displace the biotin-streptavidin probe (BSP) resulting in removing the BSP signal.

(D) The first six unfolded or partially folded events for 0 nM target oligo concentration. Most of the events have a high peaks/event ratio. Baseline current values range from 8.21 to 8.56 nA, and current trace RMS = 7.7 pA, 8.6 pA, 8.3 pA, 14.8 pA, 14.8 pA, 9.9 pA, respectively.

(E) The first six unfolded or partially folded events for 250 nM target oligo concentration. Most of the probes are displaced as indicated in a fewer peaks/event ratio. Baseline current values range from 9.92 to 9.94 nA, and current traces RMS = 13.4 pA, 31.6 pA, 9.9 pA, 15.0 pA, 15.0 pA, 15.0 pA, respectively.

(F) The relationship between oligo concentration and peaks ratio; as the concentration of oligo increases, the ratio of peaks to events decreases.

(G) The effect of storage on concentration measurements. Two-weeks-old chip was compared to a newly made fresh chip. The data show a decrease in the ratio after storage and repeated usage.

(H) The effect of baseline RMS on peaks ratio at 250 nM oligo concentration. As baseline RMS increases, the peaks ratio increases due to lower SNR (Figure S1D). Error bars correspond to the SE of the mean (±SEM). The buffer used in all experiments is 4 M LiCl, one x TE, pH ~ 9.4.

between RMS and peaks ratio was investigated, the results show that with high baseline RMS the peaks ratio increases (Figure 4H). The increase of RMS in the baseline results in producing noise signals within a DNA translocation that appears like a secondary peak. These random fluctuations explain the increase

in peaks ratio to the higher baseline RMS. Another issue with high baseline RMS is the difficulty to distinguish between primary and secondary ionic signals.

In summary, nanopores assembled into a chip can be sustained over up to 19 weeks. Our nanopore assembly into a PDMS chip in combination with the washing and storage process can help in maintaining nanopore functionality for months without any modification or coating. Nanopore characteristics, including having a linear IV relationship, and a baseline RMS below 8 pA are crucial for biosensing applications using DNA carriers with designed binding sites. High DNA carrier signal distinguishability from noise can be achieved with lower current and baseline RMS, and repeated usage of nanopores increases both values. Repeatedly used nanopores can still produce reliable measurements, but further optimization is needed to reduce the potential errors from repeated usage and possible contamination from prior samples.

Limitations of the study

Seven chips were made by one researcher over a few days. Further replication by another researcher of the nanopore fabrication, the chip assembly, and the cleaning and storage protocol would produce more significant results. The concentration measurements were done in control solutions; further experiments on biological samples would be important to determine the feasibility of nanopores for clinical biosensing. The set-up used is specific to glass conical nanopores; thus, the parameters mentioned might not apply to other types of nanopores or different set-ups. Skills of fabricating nanopores, chips assembly, and wetting nanopores can also influence reusability and stability. Operational conditions can be different among labs, and this needs to be taken into account.

STAR★METHODS

Detailed methods are provided in the online version of this paper and include the following:

- KEY RESOURCES TABLE
- RESOURCE AVAILABILITY
  - Lead contact
  - Materials availability
  - Data and code availability
- METHOD DETAILS
  - Chip fabrication
  - DNA carrier synthesis and preparation
  - Nanopore measurement
  - Storage, cleaning, and sealing process
- QUANTIFICATION AND STATISTICAL ANALYSIS

SUPPLEMENTAL INFORMATION

Supplemental information can be found online at https://doi.org/10.1016/j.isci.2022.104191.

ACKNOWLEDGMENTS

We thank the lab of Mark Howarth at Oxford University for kindly providing monovalent streptavidin. Funding: M.A. was supported by the UK Engineering and Physical Sciences Research Council (EPSRC) grant EP/S023046/1 for the Sensor CDT. M.A. acknowledges funding from UKSACB scholarship. K.C. and U.F.K. acknowledge funding from an ERC Consolidator Grant (Designerpores No. 647144). J.Z. acknowledges funding from an EPSRC grant (EP/M008258/1). F.B. acknowledges funding from George and Lilian Schiff Foundation Studentship, the Winton Programme for the Physics of Sustainability, and St John's Benefactors' Scholarship. S.E.S. acknowledges funding from the EPSRC Cambridge NanoDTC, EP/S022953/1.

AUTHOR CONTRIBUTIONS

Conceptualization, U.F.K., M.A., and F.B.; Methodology, U.F.K., M.A., and F.B.; Validation, S.S.; Formal Analysis, M.A.; Investigation, M.A.; Resources, M.A. and F.B.; Writing – Original Draft, M.A.; Writing – Review & Editing, U.F.K., M.A., F.B., K.C., J.Z., and S.S.; Visualization, M.A.; Supervision, U.F.K.

DECLARATION OF INTERESTS

U.F.K., K.C., and M.A. are founders of Cambridge Nucleomics. Other authors do not have competing interests.

Received: August 13, 2021
Revised: February 16, 2022
Accepted: March 30, 2022
Published: May 20, 2022

REFERENCES

Albrecht, T. (2017). Progress in single-biomolecule analysis with solid-state nanopores. Curr. Opin. Electrochemistry *4*, 159–165. https://doi.org/10.1016/j.coelec.2017.09.022.

Awasthi, S., Sriboonpeng, P., Ying, C., Houghtaling, J., Shorubalko, I., Marion, S., Davis, S.J., Sola, L., Chiari, M., Radenovic, A., and Mayer, M. (2020). Polymer coatings to minimize protein adsorption in solid-state nanopores. Small Methods *4*, 2000177. https://doi.org/10.1002/smtd.202000177.

Beamish, E., Tabard-Cossa, V., and Godin, M. (2020). Digital counting of nucleic acid targets using solid-state nanopores. Nanoscale *12*, 17833–17840. https://doi.org/10.1039/D0NR03878D.

Bell, N.A., and Keyser, U.F. (2016). Digitally encoded DNA nanostructures for multiplexed, single-molecule protein sensing with nanopores. Nat. Nanotechnol. *11*, 645–651. https://doi.org/10.1038/nnano.2016.50.

Bell, N.A., Thacker, V.V., Hernández-Ainsa, S., Fuentes-Perez, M.E., Moreno-Herrero, F., Liedl, T., and Keyser, U.F. (2013). Multiplexed ionic current sensing with glass nanopores. Lab Chip *13*, 1859–1862. https://doi.org/10.1039/C3LC50069A.

Bezrukov, S.M. (2000). Ion channels as molecular Coulter counters to probe metabolite transport. J. Membr. Biol. *174*, 1–13. https://doi.org/10.1007/s002320001026.

Cai, S., Pataillot-Meakin, T., Shibakawa, A., Ren, R., Bevan, C.L., Ladame, S., Ivanov, A.P., and Edel, J.B. (2021). Single-molecule amplification-free multiplexed detection of circulating microRNA cancer biomarkers from serum. Nat. Commun. *12*, 1–12. https://doi.org/10.1038/s41467-021-23497-y.

Charron, M., Briggs, K., King, S., Waugh, M., and Tabard-Cossa, V. (2019). Precise DNA concentration measurements with nanopores by controlled counting. Anal. Chem. *91*, 12228–12237. https://doi.org/10.1021/acs.analchem.9b01900.

Chen, K., Zhu, J., Boskovic, F., and Keyser, U.F. (2020). Nanopore-based DNA hard drives for rewritable and secure data storage. Nano Lett. *20*, 3754–3760. https://doi.org/10.1021/acs.nanolett.0c00755.

Chou, Y.C., Masih Das, P., Monos, D.S., and Drndić, M. (2020). Lifetime and stability of silicon nitride nanopores and nanopore arrays for ionic measurements. ACS Nano *14*, 6715–6728. https://doi.org/10.1021/acsnano.9b09964.

Dekker, C. (2007). Solid-state nanopores. Nat. Nanotech. *2*, 209–215. https://doi.org/10.1038/nnano.2007.27.

Howarth, M., Chinnapen, D.J., Gerrow, K., Dorrestein, P.C., Grandy, M.R., Kelleher, N.L., El-Husseini, A., and Ting, A.Y. (2006). A monovalent streptavidin with a single femtomolar biotin binding site. Nat. Methods *3*, 267–273. https://doi.org/10.1038/nmeth861.

Iqbal, S.M., Akin, D., and Bashir, R. (2007). Solid-state nanopore channels with DNA selectivity. Nat. Nanotechnol. *2*, 243–248. https://doi.org/10.1038/nnano.2007.78.

Karmi, A., Sakala, G.P., Rotem, D., Reches, M., and Porath, D. (2020). Durable, stable, and functional nanopores decorated by self-assembled dipeptides. ACS Appl. Mater. Inter. *12*, 14563–14568. https://doi.org/10.1021/acsami.0c00062.

Kong, J., Zhu, J., and Keyser, U.F. (2017). Single molecule based SNP detection using designed DNA carriers and solid-state nanopores. Chem. Commun. *53*, 436–439. https://doi.org/10.1039/C6CC08621G.

Nouri, R., Tang, Z., and Guan, W. (2019). Calibration-free nanopore digital counting of single molecules. Anal. Chem. *91*, 11178–11184. https://doi.org/10.1021/acs.analchem.9b01924.

Nilsson, J., Lee, J.R., Ratto, T.V., and Létant, S.E. (2006). Localized functionalization of single nanopores. Adv. Mater. *18*, 427–431. https://doi.org/10.1002/adma.200501991.

Roman, J., Jarroux, N., Patriarche, G., Français, O., Pelta, J., Le Pioufle, B., and Bacri, L. (2017). Functionalized solid-state nanopore integrated into a reusable microfluidic device for better stability and nanoparticle detection. ACS Appl. Mater. Inter. *9*, 41634–41640. https://doi.org/10.1021/acsami.7b14717.

Smeets, R.M., Keyser, U.F., Dekker, N.H., and Dekker, C. (2008). Noise in solid-state nanopores. Proc. Natl. Acad. Sci. *105*, 417–421. https://doi.org/10.1073/pnas.0705349105.

Smeets, R.M., Keyser, U.F., Wu, M.Y., Dekker, N.H., and Dekker, C. (2006). Nanobubbles in solid-state nanopores. Phys. Rev. Lett. *97*, 088101. https://doi.org/10.1103/PhysRevLett.97.088101.

Van den Hout, M., Hall, A.R., Wu, M.Y., Zandbergen, H.W., Dekker, C., and Dekker, N.H. (2010). Controlling nanopore size, shape and stability. Nanotechnology *21*, 115304. https://doi.org/10.1088/0957-4484/21/11/115304.

Xue, L., Yamazaki, H., Ren, R., Wanunu, M., Ivanov, A.P., and Edel, J.B. (2020). Solid-state nanopore sensors. Nat. Rev. Mater. *5*, 931–951. https://doi.org/10.1038/s41578-020-0229-6.

Zhang, D.Y., and Winfree, E. (2009). Control of DNA strand displacement kinetics using toehold exchange. J. Am. Chem. Soc. *131*, 17303–17314. https://doi.org/10.1021/ja906987s.

STAR★METHODS

KEY RESOURCES TABLE

REAGENT or RESOURCE	SOURCE	IDENTIFIER
Chemicals, peptides, and recombinant proteins		
Polydimethylsiloxane (PDMS)	Dow Corning	SYLGARD™ 184 Silicone Elastomer
Monovalent streptavidin	The lab of Mark Howarth at Oxford University	(Howarth et al., 2006)
ssDNA 7249 1mL at 100nm	Guild Biosciences	D-441-010-1mL100
EcoRI-HF	New England Biolabs	R3101T
BamHI-HF	New England Biolabs	R3136T
Critical commercial assays		
Machery-Nagel NucleoSpin Gel and PCR Clean-up kit	*Fisher Scientific UK Ltd*	12303368
Deposited data		
Raw nanopore current trace data	This paper	Available upon request
Oligonucleotides		
Oligos in below table and Table S3	Integrated DNA Technologies, Inc.	https://eu.idtdna.com/pages/products/custom-dna-rna/dna-oligos/custom-dna-oligos
Software and algorithms		
LabVIEW	NATIONAL INSTRUMENTS CORP.	_
Other		
Laser-assisted capillary puller	Sutter Instrument, USA	Sutter P-2000/F
Quartz glass capillaries with filament O.D.:0.50mm, I.D.:0.20mm 7cm length	Sutter Instrument, USA	QF050-20-7
Amplifier	Molecular Devices	Axopatch 200B amplifier
8-pole low pass Bessel filter	Frequency Devices INC	Model 900L8L
Data card	National Instruments	PCI-6251
Amicon ultra centrifugal filters 100K 0.5 mL	Merck Millipore Ltd.	Cat No: UFC5100BK

RESOURCE AVAILABILITY

Lead contact

Further information and requests for resources should be directed to and will be fulfilled by the lead contact, Ulrich F. Keyser (ufk20@cam.ac.uk).

Materials availability

This study did not generate new unique reagents

Data and code availability

All original raw and processed data, processing and analysis LabVIEW software, and additional information required to reanalyze the data reported in this paper are available from the lead contact upon request.

METHOD DETAILS

Chip fabrication

Glass nanopores were fabricated with a laser-assisted capillary puller (Sutter P-2000/F, Sutter Instrument, USA) using quartz capillaries with an inner diameter of 0.2 mm and an outer diameter of 0.5 mm that contains a fused filament (Sutter Instrument, USA) (Bell et al., 2013). Three different parameters were used to

make nanopores of sizes ranging from 11–18 nm (see below table). 3D printed mold was used to make polydimethylsiloxane (PDMS) (Dow Corning) chips. 1:10 curing agent to elastomer was mixed and poured on the mold, then baked at 60°C for 2 hours. 1214 nanopores were placed in grooves within the PDMS chip, then was plasma etched for 12 seconds to bound on a glass microscope slide. To prevent leakage through the chip grooves, the same PDMS ratio was used to fill them, then the chip was baked at 120°C for 30 minutes to cure PDMS. The chip was cleaned by plasma etching for 5 minutes then all chambers were filled immediately with 4 M LiCl, 1 x TE, pH ~ 9.4 then chips were stored until measurements.

Capillary pulling programs

Program	Heat	Velocity	Delay (msec)	Pull
1	480	25	170	200
2	490	25	170	200
3	500	25	170	200

Three different Sutter P-2000/F pulling parameters were used throughout the experiment. One and two were used for the nanopore lifetime experiment. Two and three were used for concentration quantification measurements.

DNA carrier synthesis and preparation

M13mp18 ssDNA (7249 bases, D-441-010-1mL100, Guild Biosciences) was linearized before hybridizing (Bell and Keyser, 2016). Circular M13mp18 ssDNA was linearized by hybridizing a 39 nucleotides (nt) ssDNA oligo (5′-TCTAGAGGATCCCCGGGTACCGAGCTCGAATTCGTAATC-3′) then it was cut using the following reaction mixture: i) 40 μL M13mp18 ssDNA (250ng/μL), 8 μL 10x Cutsmart buffer (New England Biolabs), 2 μL of the 39 nt the oligo (100μM) and 28 μL deionized water; ii) then the mixture was heated to 65°C and linearly cooled to 25°C in a thermocycler over 40 minutes; iii) 1 μL of BamHI-HF and 1 μL EcoRI-HF were added (100000 units/ml, New England Biolabs); and iv) then incubated at 37°C for 1 hour. Linear M13mp18 was purified with a Machery-Nagel NucleoSpin Gel and PCR Clean-up kit before measuring its concentration with NanoDrop.

The DNA carrier was made by the hybridizing M13mp18 ssDNA with designed 190 complementary short ssDNA (staples) (Bell and Keyser, 2016; Chen et al., 2020). To produce two peaks at asymmetrical locations, 2 groups of 6 x DNA dumbbells replacing staples sites 26–30 and 106–112 (Table S3) were hybridized at two designated locations instead of the original staples.

To make the DNA carrier the following mixture was made; linearized M13mp18 ssDNA was added to a final concentration of 25nM, 20 μL oligonucleotide mixture that includes dumbbells for nanopore lifetime experiment, and 16 nt biotin-oligo for the short oligo concentration measurements (all staple oligos were at 200 nM), 4 μL 100 mM MgCl2, 1.2 μL 100 mM Tris-EDTA (pH = 8) and filled until 40 μL deionized water. Then in a thermocycler, the reaction was heated to 70°C followed by a linear cooling to 25°C for 50 minutes to anneal the DNA carrier. Excess oligonucleotides were removed using Amicon Ultra 100 kDa filters by mixing all reaction mixture with 460 μL of 10mM Tris-HCl (pH = 8), 0.5 mM MgCl2, and then centrifuged at 9000 g for 10 minutes at 4°C. The reaction was washed again with 460 μL more 10mM Tris-HCl (pH = 8), 0.5 mM MgCl2 then centrifuged for 10 minutes. The sample was recovered by turning the filter upside down and centrifuging for 1 minute at 1000 g in a new tube. ~25 μL at a concentration of ~30–50 ng/μL is typically recovered from the reaction.

For the biosensing DNA carrier, five designed 63 nt oligos (oligo 2–6, see below table) with target binding overhang and M13 binding domain were designed to replace the original M13mp18 staples at sites 42, 55, 68, 81, and 95.

The sequences of oligos for biosensing

Oligo name	Sequence (5′ - 3′)	Length (nt)	Complementary site on M13
1	ACCACTAATG AGTGATATCC	20	_
2	TTCGACAACTCGTATTAAATCCTTTGCCCGAACGTTAT TTTTT GGATATCACT CATTAGTGGT	63	42

(*Continued on next page*)

Continued

Oligo name	Sequence (5′ - 3′)	Length (nt)	Complementary site on M13
3	GTGAGTGAATAACCTTGCTTCTGTAAATCGTCGCTATT TTTTT GGATATCACT CATTAGTGGT	63	55
4	AGAATATAAAGTACCGACAAAAGGTAAAGTAATTCTGT TTTTT GGATATCACT CATTAGTGGT	63	68
5	TCCCAATCCAAATAAGAAACGATTTTTTGTTTAACGTC TTTTT GGATATCACT CATTAGTGGT	63	81
6	GAAATTATTCATTAAAGGTGAATTATCACCGTCACCGA TTTTT GGATATCACT CATTAGTGGT	63	95
7	AATGAGTGATATCC/3-bio/	14	_

Oligo one is the target DNA strand. Oligo two to six are used to replace staples 42, 55, 68, 81, and 95 (Bell and Keyser, 2016) at the five sensing sites. Oligo seven is the 14 nt biotin-labeled DNA probe

Nanopore measurement

For nanopore lifetime measurements, DNA samples were diluted in 4 M LiCl, 1 x TE, pH ~ 9.4 to make a DNA carrier of a concentration 0.4 nM by mixing the same volume of DNA carrier with 8 M LiCl pH~ 9.4 - (2 x TE, 410 μL 2 M LiOH), then further diluting in 4 M LiCl pH~ 9.4 - (1 x TE, 205 μL 2 M LiOH). For concentration measurements, 5 nM of biosensing DNA carrier was mixed with the target strand at the desired concentration in 1x Tris-HCl (pH 8.0) and incubated at room temperature for 3 hours before measurement. For amplifying the biotin-oligo signal, monovalent streptavidin (Howarth et al., 2006) was also added to a final concentration of 10 nM and incubated for 15 minutes at room temperature.

To measure the sample, the solution was added to the loading chamber. To connect the chip, Ag/AgCl single grounded electrode is placed in the loading chamber, and another electrode was placed in an outer chamber. To drive the DNA carrier through the nanopore, a voltage of 600 mV was applied using an Axopatch 200B amplifier (Molecular Devices), then the ionic current signal was measured. An external Bessel filter (Frequency Devices) was used to filter the signal at 50 kHz and then digitized at 1 MHz sampling rate for measurement with a data card (PCI-6251, National Instruments). LabVIEW algorithms (National Instruments) were used to collect the data and analyze it.

Storage, cleaning, and sealing process

After the chip was assembled and used, the chip's loading chamber was washed twice with 100 μL nanopore measurement buffer 4 M LiCl pH~ 9.4 - (1 x TE, 205 μL 2 M LiOH), then vacuumed sealed and stored at room temperature. Before reusing the chip, the chip's loading chamber was washed twice with the same volume of 4 M LiCl - pH 9.4 - (1 x TE, 205 μL 2 M LiOH)

QUANTIFICATION AND STATISTICAL ANALYSIS

LabVIEW customized script was used to identify individual events and was done manually to reduce the potential errors when the signal to noise ratio is low. Peaks identification for measuring oligo concentration was done manually to avoid the same problem as well. All error bars reported are standard errors of the mean (±SEM).